Macromolecules

Article

Cite This: Macromolecules 2018, 51, 8522−8529

pubs.acs.org/Macromolecules

Ultrathin Shell Layers Dramatically Influence Polymer Nanoparticle Surface Mobility

Eunsoo Kang,[†] Hojin Kim,[‡] Laura A. G. Gray,[§] Dane Christie,[§] Ulrich Jonas,[∥] Bartlomiej Graczykowski,[†] Eric M. Furst,[‡] Rodney D. Priestley,[*,§] and George Fytas[*,†]

[†]Max Planck Institute for Polymer Research, Ackermannweg 10, 55128 Mainz, Germany

[‡]Department of Chemical and Biomolecular Engineering, University of Delaware, Newark, Delaware 19716, United States

[§]Department of Chemical and Biological Engineering, Princeton University, Princeton, New Jersey 08544, United States

[∥]Macromolecular Chemistry, Department of Chemistry and Biology, University of Siegen, Adolf-Reichwein-Strasse 2, 57076 Siegen, Germany

Supporting Information

ABSTRACT: Advances in nanoparticle synthesis, self-assembly, and surface coating or patterning have enabled a diverse array of applications ranging from photonic and phononic crystal fabrication to drug delivery vehicles. One of the key obstacles restricting its potential is structural and thermal stability. The presence of a glass transition can facilitate deformation within nanoparticles, thus resulting in a significant alteration in structure and performance. Recently, we detected a glassy-state transition within individual polystyrene nanoparticles and related its origin to the presence of a surface layer with enhanced dynamics compared to the bulk. The presence of this mobile layer could have a dramatic impact on the thermal stability of polymer nanoparticles. Here, we demonstrate how the addition of a shell layer, as thin as a single polymer chain, atop the nanoparticles could completely eliminate any evidence of enhanced mobility at the surface of polystyrene nanoparticles. The ultrathin polymer shell layers were placed atop the nanoparticles via two approaches: (i) covalent bonding or (ii) electrostatic interactions. The temperature dependence of the particle vibrational spectrum, as recorded by Brillouin light scattering, was used to probe the surface mobility of nanoparticles with and without a shell layer. Beyond suppression of the surface mobility, the presence of the ultrathin polymer shell layers impacted the nanoparticle glass transition temperature and shear modulus, albeit to a lesser extent. The implication of this work is that the core−shell architecture allows for tailoring of the nanoparticle elasticity, surface softening, and glass transition temperature.

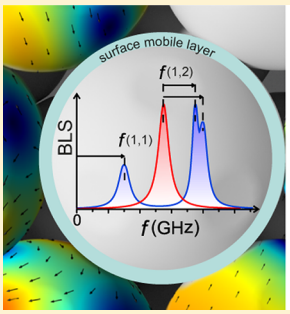

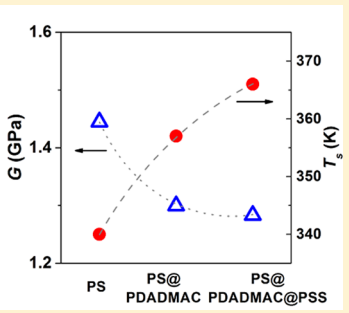

Nanomaterials made of polymer nanoparticles (NPs) have been widely studied for their unique optical and mechanical properties, which are made possible due to their nanostructure. Emerging state-of-the-art techniques for self-assembling NPs have enabled more complex structures and nucleated numerous applications including photonic[1,2] and phononic crystals,[3−5] drug delivery,[6,7] and sensing materials.[8,9] Polymer NPs are, however, thermally unstable so their performance can be easily disturbed by temperature variation resulting in structural deformation above the glass transition temperature (T_g). For instance, it has been reported that the drug release of NPs is activated by increasing the temperature near the T_g of the polymer NP carrier.[10,11] In the case of photonics applications, colloidal crystals should be treated below the T_g to prevent NPs from fusing into a consolidated film.[12] Nonetheless, mechanical properties of colloidal films composed of polymer NPs have received less attention in comparison to polymer thin films due to experimental limitations in the ability to study the temperature dependence of mechanical properties of polymer NPs.[13,14] In addition, polymer dynamics of NPs is quite complex given nanoconfinement effects and cohesive forces between adjacent polymer NPs in colloidal films.

We have recently reported that temperature-dependent Brillouin light scattering (BLS) spectroscopy can be used to estimate the shear modulus and characteristic softening temperature (T_s) of polymer NPs via analysis of their mechanical vibrational spectra.[15] Particle vibrational frequencies revealed not only the thermomechanical properties of NPs but also the adhesive forces between them. By systematically scanning the eigenfrequencies, these experiments showed the first direct experimental observation of a thermal transition well below the T_g of polystyrene (PS) NPs, which verified the

Received: August 21, 2018
Revised: October 1, 2018
Published: October 18, 2018

DOI: 10.1021/acs.macromol.8b01804
Macromolecules 2018, 51, 8522−8529

Table 1. Characteristics Dimensions for the Shell and the LbL Architecture Polymer Nanoparticles

system	shell architecture			LbL architecture[c]		
sample	PS_A	PS_A-PS	PS_A-PMMA	PS_B	PS_B@ PDADMAC	PS_B@ PDADMAC@PSS
core chemical composition	poly(styrene-*co*-acrylic acid)			poly(styrene-*co*-styrenesulfonate)		
size[a] (nm)	220 ± 7	256 ± 6	236 ± 7	167 ± 4	168 ± 4	169 ± 5
shell thickness (nm)	core	18 ± 3	8 ± 3	core	ultrathin[b]	ultrathin[b]

[a]Particle size was measured from a SEM image. [b]Physically adsorbed layer on PS_B (LbL architecture) is ultrathin, and layer thickness is in error range of SEM size measurement. Surface roughness shown by SEM images in Figure S1 confirms adsorbed polyelectrolyte layers. [c]The zeta-potential of the three NP's is plotted in Figure S2.

activation and presence of a mobile surface layer within PS NPs, as previously suggested.[16]

Based on the fundamental study of surface mobility activation, it raises a question how one can control the thermal response of polymer NPs by tuning the surface mobile layer in terms of its glass transition dynamics. Because the surface mobile layer causes enhanced polymer segmental dynamics at the interface with the surrounding medium, the resulting T_g of polymer NPs is typically reduced.[16−22] To improve the thermal stability of polymer NPs, it is crucial to control the thermal and mechanical properties of individual NPs, in addition to any adhesion between them. Here, we modify the surface of NPs with the aim to tailor the polymer surface mobility and therefore, the thermomechanical properties of individual NPs. Polystyrene core−shell structured NPs that have thin shells with different T_g values compared to the core T_g were employed to study interfacial effects on the thermomechanical properties. The thin shells were synthesized by seeded emulsion polymerization or by physical adsorption based on electrostatic interactions between the core polymer and oppositely charged polyelectrolytes in a manner similar to layer-by-layer (LbL) adsorption.[23,24] BLS was used to measure the shear modulus and softening temperature T_s, defined subsequently, of NPs assembled atop a glass substrate while T_g of the aqueous suspended NPs was measured by modulated differential scanning calorimetry (MDSC). All annealed contiguous films were compared with the corresponding NPs to understand how the structure of the shell influences (or not) surface mobility of NPs. We demonstrate that by varying the shell composition of core−shell polymer NPs that surface mobility can be tuned, which subsequently impacted NP interparticle interactions and thermal mechanical properties.

EXPERIMENTAL SECTION

Preparation of Core−Shell Nanoparticles. Two types of different polystyrene cores were used to create the shell architecture system and LbL architecture NPs. For the shell architecture system (PS_A system), we adopted styrene as a monomer and acrylic acid as a comonomer. PS_A NPs were used as the core for shell architecture NPs, PS_A-PS, and PS_A-poly(methyl methacrylate) (PMMA) core−shell NPs. All polymer suspensions were treated with a water and ethanol mixture to remove unreacted monomer and impurities before use. For the LbL architecture system (PS_B system), we used styrene as a monomer and sodium 4-vinylbenzylsulfonate (NaVBS) as a comonomer.[25] PS_B@poly(diallyldimethylammonium chloride) (PDADMAC) and PS_B@PDADMAC@poly(sodium 4-styrenesulfonate) (PSS) polyelectrolyte adsorbed nanoparticles were prepared by the layer-by-layer (LbL) polyelectrolyte adsorption method.[23,26] Briefly, 0.5 mL of PS_B NPs (0.5 vol % suspended in water) was mixed with 0.5 mL of PDADMAC (MW < 100000 g/mol) cationic polyelectrolyte (20 mg/mL in 0.5 M NaCl aqueous solution), and the mixture was vortexed for 30 min. Polyelectrolyte-coated NPs were washed by centrifugation and replacing the medium with water (Millipore Direct-Q, resistivity ρ > 18.2 MΩ·cm) followed by removal of supernatant. Particles were washed three times. For another layer of anionic polyelectrolyte PSS (MW = 70000 g/mol) layer adsorption, the same procedure was repeated. Particle diameters and shell thicknesses are listed in Table 1, and a more detailed procedure is in the Supporting Information.

Brillouin Light Scattering Spectroscopy. Brillouin light scattering (BLS) spectroscopy is applied to see direct phonon propagation in a medium. A high resolution six-pass tandem Fabry−Perot interferometer[27] provides a noncontact, nondestructive technique to examine thermally excited acoustic waves (phonons) in the gigahertz regime.[28] The scattering wave vector $\mathbf{q}$ is defined by the equation $\mathbf{q} = \mathbf{k}_s - \mathbf{k}_i$, where $\mathbf{k}_s$ and $\mathbf{k}_i$ refer to scattered and incident wave vector, respectively.[29] For transparent media, such as the present annealed films, a specific transmission geometry ($\theta = 2\alpha$) was adopted, where θ is the angle between the incident and scattered light from sample surface and α is the incident laser angle to the surface normal of the sample. In transmission geometry, $\mathbf{q}$ lies in sample plane, and the magnitude is expressed as $q = (4\pi/\lambda)\sin(\theta/2)$, where λ = 532 nm is the wavelength of the incident laser light in vacuum.[28,30]

A description of fundamental modes of vibration of elastic spheres was first presented by Lamb.[31] The vibrational modes are categorized into torsional and spheroidal modes, which are obtained from the stress-free boundary condition of a sphere surface.[32] The spheroidal mode accompanies shear and stretching motion of particle surface and causes radial displacement, while torsional mode accompanies only shear motion and no change in radial displacement. These modes are expressed in angular momentum (l) (l = 0, 1, 2, ...) and radial dependence of displacement (n) (n = 0, 1, 2, ...),[33] and those have specific frequencies inversely proportional to particle size.[34] In our study, polarized (vv) Brillouin spectra and constant wave vector q = 0.0167 nm^{-1} (at θ = 90°) are used to measure fundamental modes of vibration. Temperature is varied with a home-built temperature scanning apparatus.

Modulated Differential Scanning Calorimetry. Modulated differential scanning calorimetry (TA Instruments Q2000) was conducted to determine the glass transition temperature of the core-shell nanoparticles. Nanoparticles were either suspended in water or dried into a powder, or the dried powder was annealed overnight at 413 K to anneal the NPs into a film. In all cases, the sample was briefly heated above T_g, cooled at 10 K/min, and then heated at a rate of 20 K/min with a modulation of 0.2 K per 20 s. Table 2 reports the midpoint T_g measured on heating.

RESULTS AND DISCUSSION

Elastic Modulus and Interactions. The characteristic sizes of the shell architecture, PS_A-PS and PS_A-PMMA NPs based on PS_A core and the LbL architecture, PS_B@PDADMAC, and PS_B@PDADMAC@PSS NPs using PS_B as the core NP template are listed in Table 1. For the PS_A, acrylic acid was used as a comonomer, whereas the PS_B NPs were synthesized with sodium 4-vinylbenzenesulfonate as the comonomer. In the quasi-core−shell PS_A-PS NP, the thin PS shell was based on the same chemistry as the PS_A core. Figure 1a shows the anti-Stokes side of BLS spectra for the three shell architecture NPs (Table 1) at 294 K. To compare the (n, l)

DOI: 10.1021/acs.macromol.8b01804
Macromolecules 2018, 51, 8522−8529

Table 2. Glass Transition Temperature (T_g) for the PS Particles and PS Film with Thin Shell by BLS and MDSC[a]

	particle		bulk film	
samples	$T_{g,BLS}$ (K)	$T_{g,MDSC}$ (K)	$T_{g,BLS}$ (K)	$T_{g,MDSC}$ (K)
PS_A	366 ± 2	369 ± 1	368 ± 5	379 ± 1
PS_A-PS	366 ± 2	370 ± 1	368 ± 5	375 ± 1
PS_A-PMMA	371 ± 2	370 ± 1	368 ± 5	378 ± 1
PS_B	361 ± 2	372 ± 1	368 ± 5	383 ± 1
PS_B@PDADMAC	361 ± 2	377 ± 1	368 ± 5	382 ± 1
PS_B@PDADMAC@PSS	366 ± 2	374 ± 1	368 ± 5	382 ± 1

[a]PS bulk films for both BLS and MDSC were annealed for 14 h at 413 K.

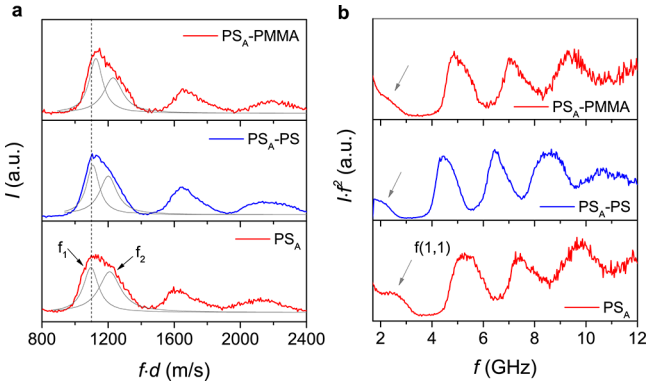

Figure 1. Brillouin light scattering (BLS) spectra of PS_A, PS_A-PS, and PS_A-PMMA nanoparticles. (a) Intensity (I) vs reduced frequency $f{\cdot}d$ (f is the frequency and d is the particle diameter) of the anti-Stokes side of the spectrum. The two line shapes (solid gray lines) indicate the representation of the (1, 2) mode by a double Lorentzian with frequencies f_1 and f_2. The vertical dotted line indicates f_1 for the PS_A nanoparticles. (b) Power spectra ($I{\cdot}f^2$) for the three nanoparticles plotted by $I{\cdot}f^2$ vs f at 294 K. The arrows indicate the interaction-induced (1, 1) mode.

bands of the spectra, the scattered light intensity (I) versus frequencies (f) was normalized by particle diameter (d), where n and l denote the radial and angular dependence of the displacement of the spheroidal modes, respectively. The Lorentzian shape representation of the $f(1,2)$ peak reveals split doublets shown by gray solid lines in Figure 1a.

The BLS spectra of Figure 1 reveal information about the intrinsic elastic properties of the nanoparticles and the strength of their interaction governed by the adhesion forces. The BLS peaks correspond to a discrete set of Lamb spheroidal modes which are further affected by the interaction with the neighboring particles. The particle−particle attractive interactions in a colloidal cluster result in a simultaneous frequency blue-shift and splitting of the particle (1, 2) mode (Figure 1a) and appearance of the low frequency (1, 1) mode (Figure 1b).[35−41] This new mode is absent in the vibration spectrum of independent, individual NP's due to its pure translational nature. The interaction-induced changes in the BLS spectrum of independent, individual NPs are schematically shown in the Table of Contents graphic, and the close packing (fcc structure) is clearly evident from the SEM images (Figure S3).

The low frequency peak of the split (1, 2) branch undergoes a blue-shift in the PS_A-PMMA NP compared to the precursor PS_A NP, as shown by the vertical dashed line in Figure 1a. To estimate the strength of the interaction-induced effect, the eigenfrequency of the (1, 2) mode for the three PS NPs, which are based on the same core, PS_A, PS_A-PS, and PS_A-PMMA, are computed using finite element method (FEM) in the absence of interactions between the NP's. In this ideal case, the (1, 2) mode corresponds to a single peak at $f(1,2)$ which is computed using a core−shell structure and elastic parameters of the bulk components. The reduced $f(1,2){\cdot}d$ value for PS_A-PMMA is the same as that for PS_A and the quasi-core−shell, PS_A-PS, thus implying a negligible influence of the 8 nm thick PMMA shell layer on the surface mobility (see Figure S4). The effective transverse sound velocity, which can be expressed by $c_t = \sqrt{G/\rho} = f(1,2){\cdot}d/A$ with the effective shear modulus (G), the mass density (ρ) of the NP, and the constant (A = 0.84 for PS), is directly computed from $f(1,2){\cdot}d$.[31] According to the FEM calculations, the PS_A-PMMA NP should have the same modulus, G = 1.5 GPa, as the precursor PS NP. However, for the former NP, the (1, 2) mode appears at higher $f(1,2){\cdot}d$ in Figure 1a.

The splitting of the peak and concurrent blue-shift of $f(1,2)$ can be attributed to adhesive forces between neighboring particles[15] enabling vibrational modes of individual NPs to resonate with each other. The (1, 1) mode is made more distinct by plotting power spectra ($I{\cdot}f^2$ against f, as shown in Figure 1b). The interparticle adhesion is described by the Johnson−Kendall−Roberts (JKR) model;[42] the factor f^2 in the power spectra accounts for the thermal population of phonons at $k_BT \gg 2\pi f\hbar$. The position of $f(1,1)$ obtained at the cutoff frequency, where the intensity is 20% of the maximum peak intensity, agrees well with the scaling law based on the JKR model: $f(1,1) \propto d^{-7/6}$ (see Figure S5), reflecting a similar adhesion energy for all PS-based NP's and further justifying the origin of the splitting of the (1, 2) mode.[15] The latter renders the calculation of the transverse sound velocity c_t (or shear modulus) from the (1, 2) mode less straightforward, but the calculation should be able to proceed through the lower f_1 and higher f_2 frequencies of the (1, 2) doublet (see Figure 1a). We have recently described the (1, 2) peak splitting and shifting behavior under adhesion and presented a new method to compute the shear modulus of NPs in colloidal clusters with

Table 3. Characteristic Particle Vibration Frequencies, Transverse Sound Velocity, and Shear Modulus of Chemically Bonded and Adsorbed Polymer Core−Shell Particles

sample	f_1 (GHz)	f_2 (GHz)	$f_L(s,1,2)$ (GHz)	$f_L(s,1,2){\cdot}d$ (m s^{-1})	c_t (m s^{-1})	G (GPa)
PS_A	4.98	5.50	4.47	983	1170	1.41
PS_A-PS	4.30	4.68	3.93	1006	1190	1.48
PS_A-PMMA	4.77	5.21	4.34	1023	1210	1.57
PS_B	6.50	7.06	5.95	994	1180	1.44
PS_B@PDADMAC	6.31	6.97	5.64	942	1120	1.30
PS_B@PDADMAC@PSS	6.38	7.16	5.61	936	1110	1.28

DOI: 10.1021/acs.macromol.8b01804
Macromolecules 2018, 51, 8522−8529

the following relation: $f_L(1,2) = 2f_1 - f_2$, where f_L refers to $f(1,2)$ of the individual NP in the case of no adhesion (see Table 3 for computed values).[15] The $f_L(1,2)$ estimated by this relation provides quite comparable f $(1,2)\cdot d$ values to the values calculated by FEM, whereas neither lower f_1 nor higher f_2 represents eigenfrequencies of free-standing NPs as shown in Figure S4. Furthermore, the $f_L(1,2)$ reveals an ~8% increase in the shear modulus of PS_A-PMMA in comparison to PS_A and PS_A-PS core−shell NP, as indicated in Figure 2. In the context

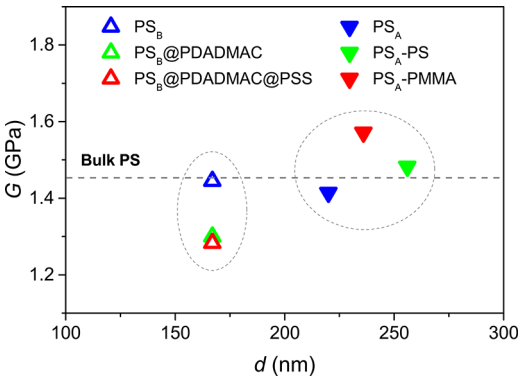

Figure 2. Shear modulus (G) of PS_A, PS_B, the shell (PS_A-PS and PS_A-PMMA), and the LbL architecture (PS_B@PDADMAC and PS_B@PDADMAC@PSS) nanoparticles. The dashed horizontal line indicates the shear modulus of bulk polystyrene.

of the FEM calculations, this higher G value suggests that either PS or PMMA in the core−shell NP should assume slightly higher density and/or c_t than in the core and shell. Given the similar G of PS_A-PS and PS_A NPs, we argue it is the thin layer of PMMA that impacts the elasticity of PS_A-PMMA NPs.

To examine the role of the shell structure in determining the mechanical vibrational modes, LbL adsorption was applied to coat one or two layers of polyelectrolyte atop PS_B NPs.[24] Two different core−shell NPs were formed using PS_B as the core NP template: (i) one layer of PDADMAC-coated atop PS_B (PS_B@PDADMAC) and (ii) one more layer of PSS-coated atop PS_B@PDADMAC (PS_B@PDADMAC@PSS). The adsorbed layers were ultrathin as indicated by SEM images (see Figure S1 and Table 1). The T_g's of the polyelectrolyte homopolymers depend critically on humidity and storage conditions. For PDADMAC and PSS, the reported T_g ranges from 297 to 443 K and from 453 to 484 K, respectively. For the PSS homopolymer's, the T_g is mostly not detectable by DSC and is estimated using the Fox equation.[43−47] Figures 3a and 3b show BLS spectra I $(f\cdot d)$ and $I\cdot f^2$ (f), respectively, for the three NP's. The change in the shape of the BLS spectra is more pronounced than for the shell architecture core−shell NPs, as shown in Figure 1, and the significant split $(f_2 - f_1)$ increases with the number of adsorbed layers through a red-shift of f_1 relative to the PS_B NP. Given the negligible thickness of each adsorbed polyelectrolyte layer (1−2 nm/layer) the observed change in the (1, 2) mode is quite significant, and it might be attributed to an enhanced adhesion between NPs.[24] Interparticle interactions are more pronounced in the frequency of the interaction-induced (1, 1) mode indicated by the arrows in Figure 3b.

Because of the negligible increase in the NP diameter through the adsorption of one or two layers of polyelectrolytes, $f(1,1)$ should be virtually that of the PS_B NP cluster. On the

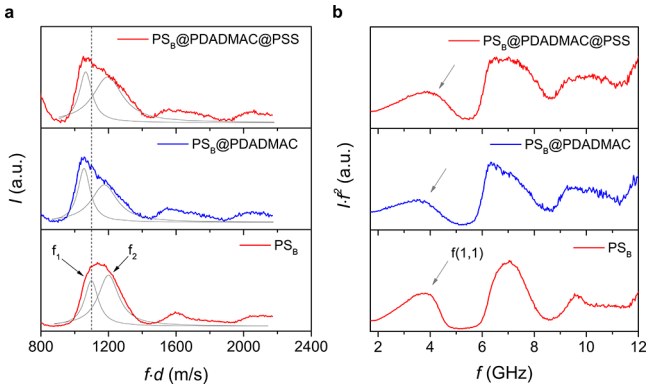

Figure 3. BLS spectra of PS_B, PS_B@PDADMAC, and PS_B@PDADMAC@PSS. (a) Intensity (I) vs reduced frequency, $f\cdot d$, of the anti-Stoke side of the spectrum. The two line shapes (solid gray lines) indicate the representation of the (1, 2) mode by a double Lorentzian with frequencies f_1 and f_2. The vertical dotted line indicates f_1 for the PS_B nanoparticles. (b) Power spectra for the three nanoparticles plotted by $I\cdot f^2$ vs f at 294 K. The arrows indicate the interaction-induced (1, 1) mode.

contrary, $f(1,1)$ systematically increases from PS_B to PS_B@PDADMAC to PS_B@PDADMAC@PSS as better seen in Figure S5. Because $f(1,1)$ is the direct representation of adhesive forces between neighboring NPs, the observed trend corroborates the notion that the existence of a thin polyelectrolyte shell promotes NPs attraction more than that of bare uncoated NPs. It further shows the sensitivity of the particle vibration spectrum to small changes in NP surface modification. However, this strong surface effect does not necessarily imply a change in the NP's shear modulus.

The shear modulus for the PS_B, PS_B@PDADMAC, and PS_B@PDADMAC@PSS can be estimated as previously from $f_L(1,2) = 2f_1 - f_2$. The computed shear moduli plotted in Figure 2 reveal a profound effect of the physical adsorption of PDADMAC and PSS on the surface of the core PS_B NP; G decreases by about 10% from that of PS_B NPs. It is a remarkably strong effect in view of the ultrathin adsorbed shell, and it could be anticipated from the red-shift of f_1 in Figure 3a. We note that an increase of G is observed when a higher modulus shell, i.e., PMMA, is chemically bound to the PS_A core (see Figure 2). We hypothesize that shell structure plays an important role in interfacial mobility, and as a result the mechanical properties of the core NPs are tunable by core−shell geometries.

Temperature Dependence of Surface Mobility and Mechanical Behavior. Temperature-dependent particle vibration spectra allow us to understand not only the thermal relaxation of polymer associated with the NP's T_g but also the surface mobility between T_s and T_g. By means of BLS, the T_g of NPs is indicated by the point where eigenmodes disappear due to the formation of a bulk polymer film. T_s is a characteristic temperature defined from the change of slope in the temperature dependence of both $f(1,2)$ (Figure 4) and $f(1,1)$ (Figure S6). The anticipated red-shift of $f(1,2)$ (decrease of c_t) with increasing temperature reverses into a blue-shift at T_s (Figure 4), whereas $f(1,1)$ abruptly increases (Figure S6) due to a significant enlargement of the contact area, in spite of no other thermal transition below T_g. This crossover T_s is assigned to the onset of surface mobility,[15] while the bulk of the NP's is still in the glassy state. Because all examined NP's and shells possess very similar T_g (Figure 5),

DOI: 10.1021/acs.macromol.8b01804
Macromolecules 2018, 51, 8522−8529

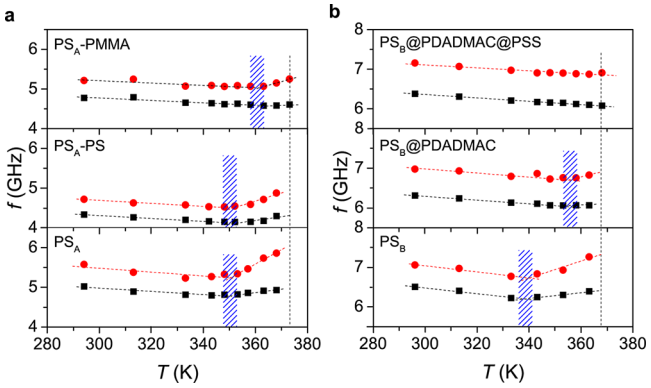

Figure 4. Temperature dependence of the frequencies f_1 and f_2 of the (1, 2) mode (Figures 1a and 3a) of (a) shell and (b) LbL architecture nanoparticles. The vertical hatched areas indicate the position of the softening transition temperature (T_s). The vertical dashed line displays the T_g of core PS_A and PS_B nanoparticles.

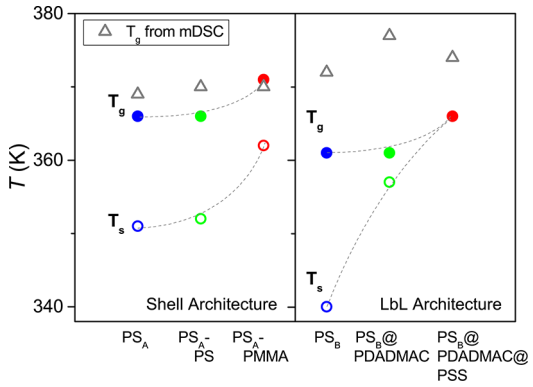

Figure 5. Effect of a thin shell on the T_s and T_g of core–shell nanoparticles. The T_s (open symbols) and T_g (closed symbols) of the shell architecture (left panel) and LbL architecture (right panel) nanoparticles are shown. Dashed line shows the trend of the T_s and T_g among the NP's. The open triangles in the two panels denote the T_g values of all six nanoparticles obtained from modulated differential scanning calorimetry in aqueous dispersions of all six nanoparticles.

the strong change of T_s is attributed to the surface modification via core–shell and LbL architectures. To exploit the relation of T_s to T_g, the core–shell architecture should involve high T_g contrast between core and shell.

Figure 4 shows $f(1,2)$ of the shell and the LbL architecture NPs, as well as their precursor core NPs (PS_A and PS_B), at elevated temperatures. Both T_s and T_g of PS_B NP at 338 and 361 K, respectively, are 5 K lower than PS_A NPs because of a different comonomer used for the synthesis. In the case of the quasi-core–shell PS_A-PS geometry, the same chemistries of the shell with the PS_A core consistently provide comparable T_s, implying that the polymerization process, necessary for the formation of the shell, does not influence T_s. Moreover, T_g of both PS_A and PS_A-PS NPs are experimentally the same, i.e., 366 ± 2 K. The formation of an 8 nm thick PMMA shell atop core PS_A NPs leads to an increase of T_g for the PS_A-PMMA NPs to 371 K. In addition, T_s of the core–shell NPs increased to 360 K, i.e., ∼10 K greater than PS_A. The increase of T_g for PS_A-PMMA NPs could be attributed to either a higher T_g of PMMA[48] and the suppression of surface mobility by the placement of the PMMA shell layer atop the NP. It effectively eliminates the free PS interface and hence the T_g confinement effect,[49] but here it is achieved by a much thinner shell. Moreover, higher T_s of PS_A-PMMA than that of PS_A and PS_A-PS is observed so it assures the fact that the surface mobility can be significantly reduced by PMMA shell with 8 nm thickness. In contrast, when capping the NPs by the physical adsorption of a polyelectrolyte shell layer, the surface mobility is shown to be strongly affected by the interactive oppositely charged polyelectrolyte layer.

As discussed earlier (see Figure 3), a PDADMAC layer capped on the PS_B NP attenuates the surface mobility because the anionic surface of the PS_B NP (due to sulfonate groups provided by potassium persulfate initiator) interacts electrostatically with the cationic PDADMAC polyelectrolyte.[24,50,51] The surface adsorption of PDADMAC polymer plays a similar role as a surfactant on a NP surface. A surfactant on the surface of NPs suppresses surface mobility, and therefore no T_g nanoconfinement effect has been reported.[17] Similarly, PS_B-PDADMAC interactions perturb the PS_B–air interface and, as a result, hinder the softening transition at the T_s of PS_B. The attenuated surface mobility of PS_B@PDADMAC results in an increase of T_s to 358 K. The detection of T_s relates to the presence of adhesive forces in colloidal clusters, as surface mobility activates adhesive forces between NPs, and the blue-shift of $f(1,2)$ with temperature above the T_s is present. Given this, for PS_B@PDADMAC NPs more thermal energy is required to promote adhesion between NPs.

One additional layer adsorption of PSS atop PS_B@PDADMAC NPs (PS_B@PDADMAC@PSS) leads to a further decrease of the surface mobility. Because one or two layers of polyelectrolytes are adsorbed in this study, we assumed that the effect of thermal shrinking or swelling depending on the outermost layer is nearly negligible.[47,52] PSS layer adsorption is based on the interaction with the PDADMAC layer, and the PSS-terminated shell is expected to form a harder shell on the core particle surface than that of PDADMAC-terminated shell.[53] The $f(1,2)$ of PS_B@PDADMAC@PSS shown in Figure 4 confirms this complete suppression of surface layer mobility. Below the NP T_g, no T_s is observed, which verifies the fact that the polyelectrolyte layer attached on the core NPs could effectively prohibit the activation of a surface mobile layer even in the presence of stronger adhesion (previous section and Figure S5). The $f(1,1)$ of PS_B@PDADMAC@PSS (see Figure S6) increases to T = 365 K which is higher than that of PS_B@PDADMAC (T_s = 358 K). Given the fact that PS NPs capped by a hard silica shell showed no T_s, it is confirmed that the shell's interaction with the surface of the core can play a similar role as hard silica capping.[54] Because typical elasticities of a silica shell fabricated by the Stöber method and PDADMAC@PSS multilayer are a few tens of GPa and a few hundreds of MPa, respectively, it corroborates the notion that the suppression of surface mobility is independent of the elasticity of shell structure.[55,56] In the case of the double layers of PDADMAC and PSS polyelectrolyte shell, which is in terms of the elasticity[55] even softer than the PS core, complete suppression of surface mobility is achieved by the electrostatically adsorbed soft shell. This independence of surface mobility and elasticity conforms to that of the glass transition behavior of polymer thin films.[57,58] Recalling the fact that the presence of charge surfactants eliminates the T_g confinement effect in NPs,[17] which is consistent with this observation, both cases can be attributed to the removal of the free surface.[59] The mechanism controlling how the charged polyelectrolytes and

DOI: 10.1021/acs.macromol.8b01804
Macromolecules 2018, 51, 8522–8529

charged surfactants impede mobility at the surface is not yet fully understood.

The systematic tuning of surface mobility, and thus the T_s, by both chemically and electrostatically fabricated core−shell NPs is shown so far as inferred by BLS. Figure 5 shows the T_s and T_g of the polymer NPs. In shell architecture core−shell NPs, their T_s and T_g increase compared to PS_A, and the amount of change of these transition temperatures depends more on the chemistries than the thickness of the shell. The robustness of T_s on the addition of 18 nm PS shell atop of PS_A core of PS_A-PS indicates that the observed strong T_s increase in PS_A-PMMA NPs is not due to chemistry effects in the interface core−shell; the quasi-core−shell PS_A-PS NPs essentially behave like a simply thicker PS NPs. The increase in T_s of PS NPs with the addition of a PMMA shell layer agrees with measurements of free-standing films of PS and PMMA, in which PS exhibits a greater T_s-confinement effect.[60,61] Physical adsorption of polyelectrolytes also affects surface mobility of the core NP as shown by the strong increase of T_s as more polyelectrolytes are adsorbed (Figure 5, right panel). We note that core−shell NPs based on electrostatic interactions have a greater influence on T_s in comparison to those based on covalent attachment, which is consistent with a greater influence of a charged shell layer on surface mobility reduction.[17,59] These observations corroborate the notion that the shell allows us to tailor the surface mobility of polymer segmental dynamics.

The T_g values of NPs measured by BLS are compared with those of MDSC using NPs suspended in water. Both NPs in air used by BLS and in water phase by MDSC are under the soft confinement condition so the extent of T_g suppression is expected to be independent for both cases.[62] According to MDSC results in Figure 5 (see Table 2 for all T_g values measured by BLS and MDSC and Figure S7 for MDSC thermograms), the T_g is varied slightly depending on the shell structure. Approximately 5 K higher T_g values of MDSC than those of BLS are consistently observed. This has been reported previously, and it was attributed to different physical mechanisms that both techniques are based on; BLS relies on the softening of the elasticity, whereas MDSC measures the relaxation of polymer segments.[15] The softening transition induced by the mobile surface layer is removed by thermal annealing of NPs above their T_g, shown in Figure S6. Forming a contiguous polymer bulk film by annealing above T_g leads to the merging of NPs and removal of individual surface layers. The absence of interfacial effects leads to the same T_g in spite of different chemistries of shell structures.

CONCLUSIONS

We studied the effect of the shell and its architecture (shell and LbL NP's) on surface mobile layer, elastic moduli, and T_g of polymer NPs using BLS and MDSC techniques. By engineering the shell of NPs, we showed that NP elasticity could be tuned via a thin shell structure either by a chemically bonded shell or by electrostatic adsorption of polyelectrolytes at room temperature. In addition to this, NPs bearing thin shells revealed the critical impact on thermal transitions of polymeric segments including T_s and T_g. When polymer colloidal films formed contiguous polymer bulk films above the T_g, the T_g values were analogous to the bulk PS T_g due to no interfacial effect of the surface mobile layer. This observation confirmed the notion that the thermomechanical properties of polymer NPs can be tailored by tuning the interfacial effects of the surface mobile layer with a core−shell structure, regardless of the thickness of the shell. We employed shell structures that show similar thermal transition behaviors as the core PS NPs in this article. A large mismatch of thermomechanical properties between core and shell may provide more dramatic changes in thermal transition and is of great interest to investigate further.

ASSOCIATED CONTENT

Supporting Information

The Supporting Information is available free of charge on the ACS Publications website at DOI: 10.1021/acs.macromol.8b01804.

Comparison between FEM calculation and experimental results, scaling relation of interaction-induced mode, SEM images of nanoparticles, temperature-dependent eigenfrequencies of polymer nanoparticles and their bulk films, and MDSC data (PDF)

AUTHOR INFORMATION

Corresponding Authors

*E-mail: fytas@mpip-mainz.mpg.de (G.F.).
*E-mail: rpriestl@princeton.edu (R.D.P.).

ORCID

Eunsoo Kang: 0000-0002-9894-0900
Ulrich Jonas: 0000-0002-2161-4541
Bartlomiej Graczykowski: 0000-0003-4787-8622
Rodney D. Priestley: 0000-0001-6765-2933

Notes

The authors declare no competing financial interest.

ACKNOWLEDGMENTS

The work was supported by ERC AdG SmartPhon (No. 694977). B.G. thanks the Alexander for Humboldt Foundation for a Fellowship. E.M.F. acknowledges support from the NASA (NNX16AD21G and NNX10AE44G) and the NSF (CBET-1637991). R.D.P. acknowledge the support of the National Science Foundation (NSF) Materials Research Science and Engineering Center Program through the Princeton Center for Complex Materials (DMR-1420541) and the AFOSR through a PECASE Award (FA9550-15-1-0017).

REFERENCES

(1) Stein, A.; Schroden, R. C. Colloidal crystal templating of three-dimensionally ordered macroporous solids: Materials for photonics and beyond. *Curr. Opin. Solid State Mater. Sci.* **2001**, *5*, 553−564.

(2) Xu, X.; Asher, S. A. Synthesis and Utilization of Monodisperse Hollow Polymeric Particles in Photonic Crystals. *J. Am. Chem. Soc.* **2004**, *126*, 7940−7945.

(3) Cheng, W.; Wang, J.; Jonas, U.; Fytas, G.; Stefanou, N. Observation and tuning of hypersonic bandgaps in colloidal crystals. *Nat. Mater.* **2006**, *5*, 830−836.

(4) Beltramo, P. J.; Schneider, D.; Fytas, G.; Furst, E. M. Anisotropic hypersonic phonon propagation in films of aligned ellipsoids. *Phys. Rev. Lett.* **2014**, *113*, 1−5.

(5) Still, T.; et al. Simultaneous occurrence of structure-directed and particle-resonance- induced phononic gaps in colloidal films. *Phys. Rev. Lett.* **2008**, *100*, 194301.

(6) Cammas, S.; et al. Thermo-responsive polymer nanoparticles with a core-shell micelle structure as site-specific drug carriers. *J. Controlled Release* **1997**, *48*, 157−164.

DOI: 10.1021/acs.macromol.8b01804
Macromolecules 2018, 51, 8522−8529

(7) Soppimath, K. S.; Aminabhavi, T. M.; Kulkarni, A. R.; Rudzinski, W. E. Biodegradable polymeric nanoparticles as drug delivery devices. *J. Controlled Release* **2001**, *70*, 1−20.
(8) Wackerlig, J.; Lieberzeit, P. A. Molecularly imprinted polymer nanoparticles in chemical sensing − Synthesis, characterisation and application. *Sens. Actuators, B* **2015**, *207*, 144−157.
(9) Canfarotta, F.; Whitcombe, M. J.; Piletsky, S. A. Polymeric nanoparticles for optical sensing. *Biotechnol. Adv.* **2013**, *31*, 1585−1599.
(10) Keurentjes, J. T. F.; et al. Externally Triggered Glass Transition Switch for Localized On-Demand Drug Delivery. *Angew. Chem., Int. Ed.* **2009**, *48*, 9867−9870.
(11) Bajpai, A. K.; Shukla, S. K.; Bhanu, S.; Kankane, S. Responsive polymers in controlled drug delivery. *Prog. Polym. Sci.* **2008**, *33*, 1088−1118.
(12) Zhang, J.; Sun, Z.; Yang, B. Self-assembly of photonic crystals from polymer colloids. *Curr. Opin. Colloid Interface Sci.* **2009**, *14*, 103−114.
(13) Voudouris, P.; et al. Anisotropic elasticity of quasi-one-component polymer nanocomposites. *ACS Nano* **2011**, *5*, 5746−5754.
(14) Cang, Y.; et al. Thermomechanical Properties and Glass Dynamics of Polymer-Tethered Colloidal Particles and Films. *Macromolecules* **2017**, *50*, 8658−8669.
(15) Kim, H.; et al. Direct observation of polymer surface mobility via nanoparticle vibrations. *Nat. Commun.* **2018**, *9*, 2918.
(16) Zhang, C.; Guo, Y.; Priestley, R. D. Glass transition temperature of polymer nanoparticles under soft and hard confinement. *Macromolecules* **2011**, *44*, 4001−4006.
(17) Feng, S.; et al. Glass transition of polystyrene nanospheres under different confined environments in aqueous dispersions. *Soft Matter* **2013**, *9*, 4614−4620.
(18) Ediger, M. D.; Forrest, J. A. Dynamics near Free Surfaces and the Glass Transition in Thin Polymer Films: A View to the Future. *Macromolecules* **2014**, *47*, 471−478.
(19) Fakhraai, Z.; Forrest, J. A. Measuring the Surface Dynamics of Glassy Polymers. *Science* **2008**, *319*, 600−604.
(20) Yang, Z.; Fujii, Y.; Lee, F. K.; Lam, C.; Tsui, O. K. C. Glass Transition Dynamics and Surface Layer Mobility in Unentangled Polystyrene Films. *Science* **2010**, *328*, 1676−1679.
(21) Keddie, J. L.; Jones, R. A. L.; Cory, R. A. Temperature in Thin Polymer Films. *Faraday Discuss.* **1994**, *98*, 219−230.
(22) Ellison, C. J.; Torkelson, J. M. The distribution of glass-transition temperatures in nanoscopically confined glass formers. *Nat. Mater.* **2003**, *2*, 695−700.
(23) Decher, G. Fuzzy Nanoassemblies: Toward Layered Polymeric Multicomposites. *Science* **1997**, *277*, 1232−1237.
(24) Caruso, F.; Lichtenfeld, H.; Donath, E.; Möhwald, H. Investigation of electrostatic interactions in polyelectrolyte multilayer films: Binding of anionic fluorescent probes to layers assembled onto colloids. *Macromolecules* **1999**, *32*, 2317−2328.
(25) Chonde, Y.; Krieger, I. M. Emulsion polymerization of styrene with ionic comonomer in the presence of methanol. *J. Appl. Polym. Sci.* **1981**, *26*, 1819−1827.
(26) Caruso, F.; Susha, A. S.; Giersig, M.; Möhwald, H. Magnetic Core−Shell Particles: Preparation of Magnetite Multilayers on Polymer Latex Microspheres. *Adv. Mater.* **1999**, *11*, 950−953.
(27) Penciu, R. S.; Kriegs, H.; Petekidis, G.; Fytas, G.; Economou, E. N. Phonons in colloidal systems. *J. Chem. Phys.* **2003**, *118*, 5224−5240.
(28) Cheng, W.; Gorishnyy, T.; Krikorian, V.; Fytas, G.; Thomas, E. L. In-Plane Elastic Excitations in 1D Polymeric Photonic Structures. *Macromolecules* **2006**, *39*, 9614−9620.
(29) Cheng, W.; et al. Phonon Dispersion and Nanomechanical Properties of Periodic 1D Multilayer Polymer Films. *Nano Lett.* **2008**, *8*, 1423−1428.
(30) Gorishnyy, T.; Ullal, C. K.; Maldovan, M.; Fytas, G.; Thomas, E. L. Hypersonic phononic crystals. *Phys. Rev. Lett.* **2005**, *94*, 115501.
(31) Lamb, H. On the Vibrations of an Elastic Sphere. *Proc. London Math. Soc.* **1882**, *s1−13*, 189−212.
(32) Duval, E.; Boukenter, A.; Champagnon, B. Vibration Eigenmodes and Size of Microcrystallites in Glass: Observation by Very-Low-Frequency Raman Scattering. *Phys. Rev. Lett.* **1986**, *56*, 2052−2055.
(33) Montagna, M. Brillouin and Raman scattering from the acoustic vibrations of spherical particles with a size comparable to the wavelength of the light. *Phys. Rev. B: Condens. Matter Mater. Phys.* **2008**, *77*, 045418.
(34) Li, Y.; et al. Micro-Brillouin scattering from a single isolated nanosphere. *Appl. Phys. Lett.* **2006**, *88*, 264107.
(35) Mattarelli, M.; Secchi, M.; Montagna, M. Phononic crystals of spherical particles: A tight binding approach. *J. Chem. Phys.* **2013**, *139*, 174710.
(36) Mattarelli, M.; Montagna, M.; Still, T.; Schneider, D.; Fytas, G. Vibration spectroscopy of weakly interacting mesoscopic colloids. *Soft Matter* **2012**, *8*, 4235−4243.
(37) Guillet, Y.; et al. All-optical ultrafast spectroscopy of a single nanoparticle-substrate contact. *Phys. Rev. B: Condens. Matter Mater. Phys.* **2012**, *86*, 035456 DOI: 10.1103/PhysRevB.86.035456.
(38) Girard, A.; et al. Mechanical coupling in gold nanoparticles supermolecules revealed by plasmon-enhanced ultralow frequency raman spectroscopy. *Nano Lett.* **2016**, *16*, 3843−3849.
(39) Ayouch, A.; et al. Elasticity of an assembly of disordered nanoparticles interacting via either Van der Waals-bonded or covalent-bonded coating layers. *ACS Nano* **2012**, *6*, 10614−10621.
(40) Poyser, C. L.; et al. Coherent acoustic phonons in colloidal semiconductor nanocrystal superlattices. *ACS Nano* **2016**, *10*, 1163−1169.
(41) Vega-Flick, A.; et al. Vibrational dynamics of a two-dimensional microgranular crystal. *Phys. Rev. B: Condens. Matter Mater. Phys.* **2017**, *96*, 024303.
(42) Johnson, K. L.; Kendall, K.; Roberts, A. D. Surface energy and the contact of elastic solids. *Proc. R. Soc. London, Ser. A* **1971**, *324*, 301−313.
(43) Lyu, X.; Clark, B.; Peterson, A. M. Thermal transitions in and structures of dried polyelectrolytes and polyelectrolyte complexes. *J. Polym. Sci., Part B: Polym. Phys.* **2017**, *55*, 684−691.
(44) Imre, Á. W.; Schönhoff, M.; Cramer, C. A conductivity study and calorimetric analysis of dried poly(sodium 4-styrene sulfonate)/poly(diallyldimethylammonium chloride) polyelectrolyte complexes. *J. Chem. Phys.* **2008**, *128*, 134905.
(45) Vidyasagar, A.; Sung, C.; Gamble, R.; Lutkenhaus, J. L. Thermal transitions in dry and hydrated layer-by-layer assemblies exhibiting linear and exponential growth. *ACS Nano* **2012**, *6*, 6174−6184.
(46) M'Bareck, C. O.; Nguyen, Q. T.; Metayer, M.; Saiter, J. M.; Garda, M. R. Poly (acrylic acid) and poly (sodium styrenesulfonate) compatibility by Fourier transform infrared and differential scanning calorimetry. *Polymer* **2004**, *45*, 4181−4187.
(47) Köhler, K.; Möhwald, H.; Sukhorukov, G. B. Thermal behavior of polyelectrolyte multilayer microcapsules: 2. Insight into molecular mechanisms for the PDADMAC/PSS system. *J. Phys. Chem. B* **2006**, *110*, 24002−24010.
(48) Feng, S.; et al. Glass transition of poly(methyl methacrylate) nanospheres in aqueous dispersion. *Phys. Chem. Chem. Phys.* **2014**, *16*, 15941−15947.
(49) Sharp, J. S.; Forrest, J. A. Free surfaces cause reductions in the glass transition temperature of thin polystyrene films. *Phys. Rev. Lett.* **2003**, *91*, 235701.
(50) Caruso, F.; Caruso, R. A.; Möhwald, H. Nanoengineering of inorganic and hybrid hollow spheres by colloidal templating. *Science* **1998**, *282*, 1111−1114.
(51) Caruso, F. Nanoengineering of particle surfaces. *Adv. Mater.* **2001**, *13*, 11−22.
(52) Köhler, K.; Shchukin, D. G.; Möhwald, H.; Sukhorukov, G. B. Thermal behavior of polyelectrolyte multilayer microcapsules. 1. The

DOI: 10.1021/acs.macromol.8b01804
Macromolecules 2018, 51, 8522−8529

effect of odd and even layer number. *J. Phys. Chem. B* **2005**, *109*, 18250−18259.
(53) Lehaf, A. M.; Hariri, H. H.; Schlenoff, J. B. Homogeneity, modulus, and viscoelasticity of polyelectrolyte multilayers by nanoindentation: Refining the buildup mechanism. *Langmuir* **2012**, *28*, 6348−6355.
(54) Still, T.; D'Acunzi, M.; Vollmer, D.; Fytas, G. Mesospheres in nano-armor: Probing the shape-persistence of molten polymer colloids. *J. Colloid Interface Sci.* **2009**, *340*, 42−45.
(55) Gao, C.; Leporatti, S.; Moya, S.; Donath, E.; Möhwald, H. Stability and mechanical properties of polyelectrolyte capsules obtained by stepwise assembly of poly(styrenesulfonate sodium salt) and poly(diallyldimethyl ammonium) chloride onto melamine resin particles. *Langmuir* **2001**, *17*, 3491−3495.
(56) Zhang, L.; et al. Hollow Silica Spheres: Synthesis and Mechanical Properties. *Langmuir* **2009**, *25*, 2711−2717.
(57) Torres, J. M.; Stafford, C. M.; Vogt, B. D. Elastic Modulus of Amorphous Polymer Thin Films: Relationship to the Glass Transition Temperature. *ACS Nano* **2009**, *3*, 2677−2685.
(58) Mirigian, S.; Schweizer, K. S. Communication: Slow relaxation, spatial mobility gradients, and vitrification in confined films. *J. Chem. Phys.* **2014**, *141*, 161103.
(59) Christie, D.; Zhang, C.; Fu, J.; Koel, B.; Priestley, R. D. Glass transition temperature of colloidal polystyrene dispersed in various liquids. *J. Polym. Sci., Part B: Polym. Phys.* **2016**, *54*, 1776−1783.
(60) Roth, C. B.; Pound, A.; Kamp, S. W.; Murray, C. A.; Dutcher, J. R. Molecular-weight dependence of the glass transition temperature of freely-standing poly(methyl methacrylate) films. *Eur. Phys. J. E: Soft Matter Biol. Phys.* **2006**, *20*, 441−448.
(61) Forrest, J. A.; Dalnoki-Veress, K.; Stevens, J. R.; Dutcher, J. R. Effect of free surfaces on the glass transition temperature of thin polymer films. *Phys. Rev. Lett.* **1996**, *77*, 2002−2005.
(62) Perez-de-Eulate, N. G.; Di Lisio, V.; Cangialosi, D. Glass transition and molecular dynamics in polystyrene nanospheres by fast scanning calorimetry. *ACS Macro Lett.* **2017**, *6*, 859−863.

DOI: 10.1021/acs.macromol.8b01804
Macromolecules 2018, 51, 8522−8529